Fault Estimation Observers for the Vehicle Suspension with a Varying Chassis Mass

Gia Quoc Bao Tran, Thanh-Phong Pham, Olivier Sename

Fault Estimation Observers for the Vehicle Suspension with a Varying Chassis Mass

Gia Quoc Bao Tran [*] **Thanh-Phong Pham** [**]
Olivier Sename [***]

[*] *Centre Automatique et Systèmes, Mines Paris - PSL, Paris, France (e-mail: gia-quoc-bao.tran@minesparis.psl.eu).*
[**] *Faculty of Electrical and Electronic Engineering, The University of Danang – University of Technology and Education, Danang, Vietnam (e-mail: ptphong@ute.udn.vn).*
[***] *Univ. Grenoble Alpes, CNRS, Grenoble INP$^{\perp}$, GIPSA-Lab, 38000 Grenoble, France ($^{\perp}$Institute of Engineering Univ. Grenoble Alpes) (e-mail: olivier.sename@grenoble-inp.fr).*

Abstract: This paper proposes a descriptor Nonlinear Parameter Varying (NLPV) observer for damper fault estimation in vehicle semi-active suspension systems, here considering the highly practical case of a varying sprung mass, which is an open problem. This mass and the control input are treated as known scheduling parameters for the design and implementation of the observers, thus making the structure adaptive. This novel modeling leads to parameter-dependent dynamics and output matrices in the nonlinear parameter-varying formulation. To solve this problem, we extend an existing reduced-order observer design method (following descriptor system modeling) to this new case. Both polytopic and grid-based methods are then considered to compute and implement the problem solutions. The designs are then assessed using frequency-domain analysis and realistic time-domain simulations.

Keywords: Nonlinear Parameter Varying, descriptor, fault estimation, semi-active suspension.

1. INTRODUCTION

The suspension is a crucial component in vehicles, serving to ensure safety via its road-holding performance as well as comfort for passengers by mitigating road disturbances. The literature on suspension research is rich, for instance (Savaresi et al., 2010; Unger et al., 2013) and the references therein. Suspensions can be divided into 3 types, namely active, passive, and semi-active (SA) suspensions, among which the SA ones are preferred thanks to their balanced trade-off between performance and energy consumption.

However, in the case of loss of effectiveness of an SA damper, a stage of fault diagnosis and fault tolerant control can be integrated, which requires us to propose extended models and fault estimation algorithms (Hernández-Alcántara et al., 2016; Morato et al., 2020; Do et al., 2020). Knowing that fault dynamics are typically unknown to observer design, two main routes have been used, including the proportional-integral (PI) one (Tran et al., 2022; Do et al., 2018; Guzman et al., 2021) assuming a slow-varying fault (Isermann, 2005), and the reduced-order observer following the descriptor formulation (Pham et al., 2022). The first one relies on a rather strict assumption that the fault is *slow-varying* and, therefore, has zero time derivatives. Consequently, the fault, which is a lost part of the damper force (see (2) below), is modeled as a constant extra state to be estimated by a PI observer (Tran et al., 2022). While this can be justified for slow faults, it is not practical for other ones. A solution to avoid this slow-variation assumption of the fault is to design observers for *descriptor* systems (merging differential and algebraic equations (Darouach et al., 2017)) as proposed in our previous work (Pham et al., 2022). One of the underlying interests is that it applies to faults of arbitrary dynamics.

However, as considered in works such as (Wen et al., 2017; Maciejewski et al., 2014), the chassis or sprung mass m_s depends in practice on the passenger number and vehicle load, which should be considered. As illustrated in (Tudón-Martínez et al., 2015) a suspension control scheme adapted to the sprung mass variation should perform better than one designed assuming a constant mass, in terms of both road-holding performance and comfort.

Remark 1. Considering fault estimation using a quarter-car model is coherent in view of monitoring each damper of the suspension system. Studying the sprung mass variations allows us to handle the unknown mass distribution of a real full-car system, and the corresponding load transfer phenomena. In this paper, it is assumed that the knowledge of the mass variations is available at all times. Note that this mass can be estimated in real time as shown in existing works (Gobbi et al., 2011; Wenzel et al., 2006).

In this work, fault estimation observers are proposed in the form of Nonlinear Parameter Varying (NLPV) systems, accounting for varying sprung mass. The main contributions of this paper are:

- Thanks to available mass estimation schemes, the sprung mass is modeled as a known parameter used

in LMI solving and observer scheduling, leading to parameter dependence in both the dynamics and the output instead of only the input matrix as in (Pham et al., 2022) which requires special attention and some specific adaptation;
- Observer parameterization is extended for this case of parameter-dependent dynamics and output matrices in Section 3. Two designs are then proposed following the polytopic and grid-based method in Section 4;
- The two designs are analyzed and compared in the frequency domain via Bode plots and the polytopic one is tested via realistic simulations.

Notations: Let $W^\top$ denote the transpose of the matrix W. Denote W^+ as any general inverse of matrix W satisfying $WW^+W = W$ and W^{-1} as the inverse of the invertible square matrix W. Last, $\hat{v}$ denotes the estimate of v.

2. THE SEMI-ACTIVE SUSPENSION SYSTEM

The Electro-Rheological (ER) suspension from (Pham et al., 2019) is given in Figure 1. It consists of the sprung mass m_s, the unsprung mass m_{us}, and the suspension components located between these masses and the tire modeled as a spring of stiffness k_t.

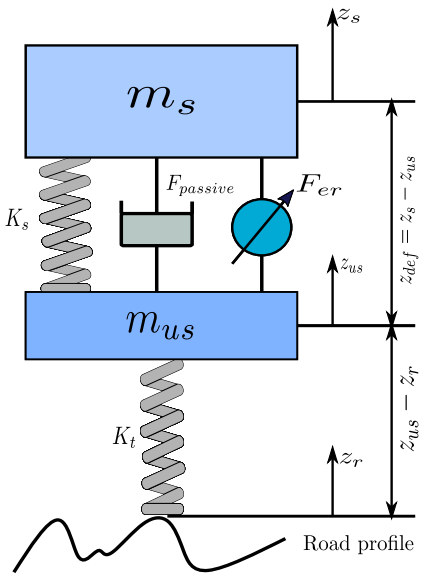

Fig. 1. Quarter-car model with a semi-active suspension.

The dynamics around the equilibrium are

$$\begin{cases} m_s\ddot{z}_s = -F_s - F_{d,f} \\ m_{us}\ddot{z}_{us} = F_s + F_{d,f} - F_t, \end{cases} \tag{1}$$

where z_s and z_{us} are the displacements of the sprung and unsprung masses, respectively; z_r is the road displacement input; $F_s = k_s z_{def}$ is the spring force ($z_{def} = z_s - z_{us}$ is the deflection); $F_t = k_t(z_{us} - z_r)$ is the tire force.

The faulty damper force $F_{d,f}$ is given in (2):

$$F_{d,f} = F_d - f, \tag{2}$$

where f is the lost damper force to be estimated and F_d is the damper force in the healthy case, as given below

$$\begin{cases} F_d = k_0 z_{def} + c_0 \dot{z}_{def} + F_{er} \\ \dot{F}_{er} = -\dfrac{1}{\tau}F_{er} + \dfrac{f_c}{\tau}\cdot u \cdot \tanh(k_1 z_{def} + c_1 \dot{z}_{def}), \end{cases} \tag{3}$$

where $u \in [0,1]$ is the control input (the electric voltage supplied to the ER damper). Substituting (2) into (1), we obtain the system dynamics considering the loss of effectiveness of the damper

$$\begin{cases} m_s\ddot{z}_s = -F_s - F_d + f \\ m_{us}\ddot{z}_{us} = F_s + F_d - f - F_t. \end{cases} \tag{4}$$

Since the sprung mass m_s is considered varying but still remaining between known bounds, i.e., $\underline{m}_s \le m_s \le \overline{m}_s$, and u is a known input, we choose the scheduling vector $\rho = (\rho_1, \rho_2)$, where $\rho_1 = \frac{1}{m_s} \in \left[\frac{1}{\overline{m}_s}, \frac{1}{\underline{m}_s}\right]$ and $\rho_2 = u \in [0,1]$, that is assumed to be known and to remain at all times in the compact set $\mathcal{P} := \left[\frac{1}{\overline{m}_s}, \frac{1}{\underline{m}_s}\right] \times [0,1]$. We assume that $\underline{m}_s = 2.2$kg and $\overline{m}_s = 2.4$kg, which is coherent with the 1/5th-scale quarter-car model at GIPSA-Lab.

Choosing the state vector as $x = (x_1, x_2, x_3, x_4, x_5, x_6) = (z_s - z_{us}, \dot{z}_s, z_{us} - z_r, \dot{z}_{us}, F_{er}, f) \in \mathbb{R}^6$, the system dynamics satisfy the descriptor NLPV form:

$$\mathcal{S}(\rho): \begin{cases} E\dot{x} = A(\rho)x + B(\rho)\Phi(x) + D_r\omega \\ y = C(\rho)x + D_n\omega, \end{cases} \tag{5}$$

where $y = (y_1, y_2) = (\ddot{z}_s, \ddot{z}_{us}) \in \mathbb{R}^2$ is the measurement and $\omega = (\dot{z}_r, \omega_n) \in \mathbb{R}^2$ with $\dot{z}_r$ the road profile derivative and ω_n the sensor noise.

The system nonlinearity is $\Phi(x) = \tanh(k_1 x_1 + c_1(x_2 - x_4)) = \tanh(\Gamma x)$, with $\Gamma = (k_1 \ c_1 \ 0 \ -c_1 \ 0 \ 0)$, and is globally Lipschitz, i.e.,

$$\|\Phi(x) - \Phi(\hat{x})\| \le \|\Gamma(x - \hat{x})\|, \quad \forall (x, \hat{x}) \in \mathbb{R}^6 \times \mathbb{R}^6. \tag{6}$$

The system matrices are then (with $k = k_s + k_0$)

$$A(\rho) = \begin{pmatrix} 0 & 1 & 0 & -1 & 0 & 0 \\ -k\rho_1 & -c_0\rho_1 & 0 & c_0\rho_1 & -\rho_1 & \rho_1 \\ 0 & 0 & 0 & 1 & 0 & 0 \\ \frac{k}{m_{us}} & \frac{c_0}{m_{us}} & \frac{-k_t}{m_{us}} & \frac{-c_0}{m_{us}} & \frac{1}{m_{us}} & \frac{-1}{m_{us}} \\ 0 & 0 & 0 & 0 & \frac{-1}{\tau} & 0 \end{pmatrix}, B(\rho) = \begin{pmatrix} 0 \\ 0 \\ 0 \\ 0 \\ \frac{f_c}{\tau}\rho_2 \end{pmatrix},$$

$$D_r = \begin{pmatrix} 0 & 0 \\ 0 & 0 \\ -1 & 0 \\ 0 & 0 \\ 0 & 0 \end{pmatrix}, D_n = \begin{pmatrix} \overline{D}_n \\ \underline{D}_n \end{pmatrix} = \begin{pmatrix} 0 & 10^{-2} \\ 0 & 10^{-3} \end{pmatrix}, E = \begin{pmatrix} I & 0 \end{pmatrix},$$

$$C(\rho) = \begin{pmatrix} C_{y,1}(\rho) \\ C_{y,2} \end{pmatrix} = \begin{pmatrix} -k\rho_1 & -c_0\rho_1 & 0 & c_0\rho_1 & -\rho_1 & \rho_1 \\ \frac{k}{m_{us}} & \frac{c_0}{m_{us}} & \frac{-k_t}{m_{us}} & \frac{-c_0}{m_{us}} & \frac{1}{m_{us}} & \frac{-1}{m_{us}} \end{pmatrix}.$$

Remark 2. We could define a loss-of-efficiency factor as $\alpha = f/F_d$ (when $F_d \neq 0$). From the estimated additive fault and damper force, we can estimate this factor as $\hat{\alpha} = \hat{f}/\hat{F}_d$ (when $\hat{F}_d \neq 0$), where

$$\hat{F}_d = k_0\hat{x}_1 + c_0(\hat{x}_2 - \hat{x}_4) + \hat{x}_5. \tag{7}$$

3. OBSERVER PARAMETERIZATION

3.1 System Modeling and Observer Formulation

Thanks to our selection of ρ, both the dynamics and output matrices are affine in ρ. In order to use a single framework for both the *polytopic* and the *grid-based* methods, C must be made independent of ρ by adding a filter with state $\chi \in \mathbb{R}$ and output $y_\chi \in \mathbb{R}$, *only* at the first output y_1 of (5):

$$\begin{cases} \dot{\chi} = A_\chi \chi + B_\chi y_1 \\ y_\chi = C_\chi \chi. \end{cases} \tag{8}$$

We can take for example $C_\chi = 1$ and $-A_\chi = B_\chi >> 1$ so that χ or y_χ converges very fast to y_1. Then, y_χ replaces y_1 as part of the output $y_{\text{ext}} = (y_\chi, y_2) \in \mathbb{R}^2$ of the extended system with state $x' := (\chi, x) \in \mathbb{R}^7$ and dynamics:

$$\mathcal{S}'(\rho) : \begin{cases} E'\dot{x}' = A'(\rho)x' + B'(\rho)\Phi'(x') + D'_r\omega \\ y_{\text{ext}} = C'x' + D'_n\omega, \end{cases} \tag{9}$$

where $E' = \begin{pmatrix} I & 0 \\ 0 & E \end{pmatrix}$, $A'(\rho) = \begin{pmatrix} A_\chi & B_\chi C_{y,1}(\rho) \\ 0 & A(\rho) \end{pmatrix}$, $B'(\rho) = \begin{pmatrix} 0 \\ B(\rho) \end{pmatrix}$, $D'_r = \begin{pmatrix} B_\chi \overline{D}_n \\ D_r \end{pmatrix}$, $C' = \begin{pmatrix} C_\chi & 0 \\ 0 & C_{y,2} \end{pmatrix}$, $D'_n = \begin{pmatrix} 0 \\ \underline{D}_n \end{pmatrix}$.

Note that $\Phi'(x') = \Phi(x)$ is globally Lipschitz with constant $\Gamma' = (0\ \Gamma)$, namely for all $(x', \hat{x}') \in \mathbb{R}^7 \times \mathbb{R}^7$,

$$\|\Phi'(x') - \Phi'(\hat{x}')\| \leq \|\Gamma'(x' - \hat{x}')\|. \tag{10}$$

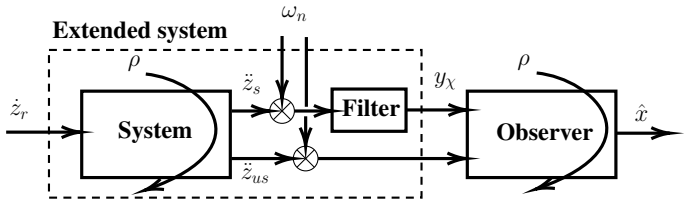

Fig. 2. Scheme of the system extension for observer design.

Remark 3. Thanks to the *descriptor* representation, there is no assumption on the fault dynamics, unlike when using a PI observer. Note also that in this case, it is not possible to filter both the two outputs, otherwise the rank conditions given in Section 3.2 would not be satisfied.

The reduced-order observer takes the form

$$\mathcal{O}(\rho) : \begin{cases} \dot{z} = N(\rho)z + J(\rho)y_{\text{ext}} + H(\rho)\Phi'(\hat{x}') \\ \hat{x}' = R(\rho)z + S(\rho)y_{\text{ext}}, \end{cases} \tag{11}$$

where $z \in \mathbb{R}^5$ is the observer state and $\hat{x}'$ is the estimate of x'. The observer matrices $N(\rho)$, $J(\rho)$, $H(\rho)$, $R(\rho)$, and $S(\rho)$ of appropriate dimensions have to be designed. Let us introduce the dynamic error

$$\epsilon = z - TE'x' \in \mathbb{R}^5, \tag{12}$$

where T is an arbitrary matrix. Differentiating (12) with respect to time and using (9) and (11), one obtains

$$\begin{cases} \dot{\epsilon} = N(\rho)\epsilon + (N(\rho)TE' - TA'(\rho) + J(\rho)C')x \\ \qquad + (H(\rho) - TB'(\rho))\Phi'(\hat{x}') \\ \qquad - TB'(\rho)(\Phi(x) - \Phi'(\hat{x}')) \\ \qquad + (J(\rho)D'_n - TD'_r)\omega \\ \hat{x}' = R(\rho)\epsilon + (R(\rho)TE' + S(\rho)C')x + S(\rho)D'_n\omega. \end{cases} \tag{13}$$

It is obvious that if the decoupling conditions

$$N(\rho)TE' - TA'(\rho) + J(\rho)C' = 0, \tag{14}$$

$$H(\rho) - TB'(\rho) = 0, \tag{15}$$

$$R(\rho)TE' + S(\rho)C' = I, \tag{16}$$

are satisfied for all $\rho \in \mathcal{P}$, system (13) becomes

$$\begin{cases} \dot{\epsilon} = N(\rho)\epsilon - TB'(\rho)\Delta\Phi' + (J(\rho)D'_n - TD'_r)\omega \\ e = R(\rho)\epsilon + S(\rho)D'_n\omega, \end{cases} \tag{17}$$

where $e := \hat{x}' - x'$ is the error and $\Delta\Phi' = \Phi'(x') - \Phi'(\hat{x}')$. We also define $e_f := f - \hat{f} = C_w e$ with a weighting matrix

$$C_w = (0\ 0\ 0\ 0\ 0\ 0\ 1)$$

to emphasize the attenuation of disturbance/noise on the fault estimation error. Parameterization of the observer matrices is next performed to satisfy the decoupling conditions (14)-(16).

3.2 Observer Parameterization

This part is extended from our former work (Pham et al., 2022), considering parameter-dependent matrices $R(\rho)$ and $S(\rho)$. First note that from (15), we get for all $\rho \in \mathcal{P}$

$$H(\rho) = TB'(\rho). \tag{18}$$

Therefore, $H(\rho)$ will be determined once T is chosen. Parameterization is made by using the general solution of (14) and (16). First, from (14) and (16), one obtains for all $\rho \in \mathcal{P}$,

$$\begin{pmatrix} N(\rho) & J(\rho) \\ R(\rho) & S(\rho) \end{pmatrix} \begin{pmatrix} TE' \\ C' \end{pmatrix} = \begin{pmatrix} TA'(\rho) \\ I \end{pmatrix}. \tag{19}$$

The equation (19) is solvable if and only if for all $\rho \in \mathcal{P}$,

$$\operatorname{rank} \begin{pmatrix} TE' \\ C' \\ TA'(\rho) \\ I \end{pmatrix} = \operatorname{rank} \begin{pmatrix} TE' \\ C' \end{pmatrix} = 7, \tag{20}$$

which is satisfied in our case. Let Υ be an arbitrary matrix of full row rank such that

$$\operatorname{rank} \begin{pmatrix} \Upsilon \\ C' \end{pmatrix} = \operatorname{rank} \begin{pmatrix} TE' \\ C' \end{pmatrix} = 7. \tag{21}$$

Then there always exists a parameter matrix K such that

$$\begin{pmatrix} TE' \\ C' \end{pmatrix} = \begin{pmatrix} I & -K \\ 0 & I \end{pmatrix} \begin{pmatrix} \Upsilon \\ C' \end{pmatrix} \iff TE' = \Upsilon - KC'$$

$$\iff (T\ K) \begin{pmatrix} E' \\ C' \end{pmatrix} = \Upsilon. \tag{22}$$

A solution for (22) is given by $(T\ K) = \Upsilon\Sigma^+$ where $\Sigma = \begin{pmatrix} E' \\ C' \end{pmatrix}$. This is equivalent to

$$T = \Upsilon\Sigma^+ \begin{pmatrix} I \\ 0 \end{pmatrix}, \qquad K = \Upsilon\Sigma^+ \begin{pmatrix} 0 \\ I \end{pmatrix}. \tag{23}$$

Note that it is required that $\operatorname{rank}\Sigma = 7$ (Delshad et al., 2016), which is satisfied in our case. The family of solutions of (19) is given by

$$\begin{pmatrix} N(\rho) & J(\rho) \\ R(\rho) & S(\rho) \end{pmatrix} = \begin{pmatrix} TA'(\rho) \\ I \end{pmatrix} \begin{pmatrix} TE' \\ C' \end{pmatrix}^+ + \begin{pmatrix} \boldsymbol{Z_1}(\rho) \\ \boldsymbol{Z_2}(\rho) \end{pmatrix} \left(I - \begin{pmatrix} TE' \\ C' \end{pmatrix} \begin{pmatrix} TE' \\ C' \end{pmatrix}^+ \right), \tag{24}$$

where $\begin{pmatrix} \boldsymbol{Z_1}(\rho) \\ \boldsymbol{Z_2}(\rho) \end{pmatrix}$ is an arbitrary matrix of appropriate dimension. This is equivalent to

$$N(\rho) = TA'(\rho)\alpha_1 + \boldsymbol{Z_1}(\rho)\beta_1, \tag{25}$$

$$J(\rho) = TA'(\rho)\alpha_2 + \boldsymbol{Z_1}(\rho)\beta_2, \tag{26}$$

$$R(\rho) = \alpha_1 + \boldsymbol{Z_2}(\rho)\beta_1, \tag{27}$$

$$S(\rho) = \alpha_2 + \boldsymbol{Z_2}(\rho)\beta_2, \tag{28}$$

with

$$\alpha_1 = \begin{pmatrix} TE' \\ C' \end{pmatrix}^+ \begin{pmatrix} I \\ 0 \end{pmatrix},\ \beta_1 = \left(I - \begin{pmatrix} TE' \\ C' \end{pmatrix} \begin{pmatrix} TE' \\ C' \end{pmatrix}^+ \right) \begin{pmatrix} I \\ 0 \end{pmatrix},$$

$$\alpha_2 = \begin{pmatrix} TE' \\ C' \end{pmatrix}^+ \begin{pmatrix} 0 \\ I \end{pmatrix},\ \beta_2 = \left(I - \begin{pmatrix} TE' \\ C' \end{pmatrix} \begin{pmatrix} TE' \\ C' \end{pmatrix}^+ \right) \begin{pmatrix} 0 \\ I \end{pmatrix}.$$

System (17) is now re-written as

$$\begin{cases} \dot{\epsilon} = \mathbb{A}(\rho)\epsilon + \mathbb{W}(\rho)\Delta\Phi' + \mathbb{B}(\rho)\omega \\ e = \mathbb{C}(\rho)\epsilon + \mathbb{D}(\rho)\omega, \end{cases} \tag{29}$$

where

$$\mathbb{A}(\rho) = N(\rho) = A_1(\rho) + \boldsymbol{Z_1}(\rho)A_2, \tag{30}$$
$$\mathbb{W}(\rho) = -TB'(\rho), \tag{31}$$
$$\mathbb{B}(\rho) = J(\rho)D'_n - TD'_r = B_1(\rho) + \boldsymbol{Z_1}(\rho)B_2, \tag{32}$$
$$\mathbb{C}(\rho) = R(\rho) = C_1 + \boldsymbol{Z_2}(\rho)C_2, \tag{33}$$
$$\mathbb{D}(\rho) = S(\rho)D'_n = D_1 + \boldsymbol{Z_2}(\rho)D_2, \tag{34}$$

where $A_1(\rho) = TA'(\rho)\alpha_1$, $A_2 = \beta_1$, $B_1(\rho) = TA'(\rho)\alpha_2 D'_n - TD'_r$, $B_2 = \beta_2 D'_n$, $C_1 = \alpha_1$, $C_2 = \beta_1$, $D_1 = \alpha_2 D'_n$, and $D_2 = \beta_2 D'_n$. Note that all the matrices $A_1(\rho)$, A_2, $B_1(\rho)$, B_2, C_1, C_2, D_1, and D_2 are known.

Therefore, the observer design problem is reduced to finding $\boldsymbol{Z_1}(\rho)$ and $\boldsymbol{Z_2}(\rho)$, which is discussed in the following part. Then, the observer matrices are computed from (18) and (25)-(28).

4. LMI-BASED OBSERVER DESIGNS

4.1 Polytopic Design

In this part, a reduced-order observer is proposed for system (9) following the *polytopic* method. In this method, the observer matrices are solved only at the vertices of the polytope formed by the variation of ρ in $\mathcal{P}$. Theorem 1 below proposes an LMI framework for the polytopic observer design.

Theorem 1. The polytopic reduced-order observer design problem is solved if given some $\boldsymbol{\kappa} > 0$, there exist matrices $\boldsymbol{X} = \boldsymbol{X}^\top > 0$, $\boldsymbol{Y}(\varrho_i)$, and $\boldsymbol{Z_2}(\varrho_i)$ minimizing $\boldsymbol{\gamma^2}$ such that for all the vertices $\varrho_i, i = 1,2,3,4$ of the polytope formed by the variation of ρ in $\mathcal{P}$,

$$\begin{pmatrix} \Omega_{11}(\varrho_i) & \boldsymbol{X}\mathbb{W}(\varrho_i) & \Omega_{13}(\varrho_i) & \Omega_{14}(\varrho_i) & \Omega_{15}(\varrho_i) \\ \star & -\boldsymbol{\kappa}I & 0 & 0 & 0 \\ \star & \star & -\boldsymbol{\gamma^2}I & \Omega_{34}(\varrho_i) & \Omega_{35}(\varrho_i) \\ \star & \star & \star & -I & 0 \\ \star & \star & \star & \star & -\boldsymbol{\kappa}I \end{pmatrix} < 0, \tag{35a}$$

where

$$\Omega_{11}(\varrho_i) = A_1^\top(\varrho_i)\boldsymbol{X} + \boldsymbol{X}A_1(\varrho_i) + A_2^\top \boldsymbol{Y}^\top(\varrho_i) + \boldsymbol{Y}(\varrho_i)A_2, \tag{35b}$$
$$\Omega_{13}(\varrho_i) = \boldsymbol{X}B_1(\varrho_i) + \boldsymbol{Y}(\varrho_i)B_2, \tag{35c}$$
$$\Omega_{14}(\varrho_i) = C_1^\top C_w^\top + C_2^\top \boldsymbol{Z_2}^\top(\varrho_i)C_w^\top, \tag{35d}$$
$$\Omega_{15}(\varrho_i) = \boldsymbol{\kappa}(C_1^\top \Gamma'^\top + C_2^\top \boldsymbol{Z_2}^\top(\varrho_i)\Gamma'^\top), \tag{35e}$$
$$\Omega_{34}(\varrho_i) = D_1^\top C_w^\top + D_2^\top \boldsymbol{Z_2}^\top(\varrho_i)C_w^\top, \tag{35f}$$
$$\Omega_{35}(\varrho_i) = \boldsymbol{\kappa}(D_1^\top \Gamma'^\top + D_2^\top \boldsymbol{Z_2}^\top(\varrho_i)\Gamma'^\top). \tag{35g}$$

Then, $\boldsymbol{Z_1}(\rho)$ at each vertex is $\boldsymbol{Z_1}(\varrho_i) = \boldsymbol{X}^{-1}\boldsymbol{Y}(\varrho_i)$, $i = 1,2,3,4$.

Proof. Consider the Lyapunov function $V(\epsilon) = \epsilon^\top \boldsymbol{X}\epsilon$, where $\boldsymbol{X} = \boldsymbol{X}^\top > 0$. Differentiating V along the solutions of (29) and denoting $\eta = (\epsilon, \Delta\Phi', \omega)$ yield

$$\begin{aligned}\dot{V}(\eta,\rho) &= \epsilon^\top \left(\mathbb{A}^\top(\rho)\boldsymbol{X} + \boldsymbol{X}\mathbb{A}(\rho)\right)\epsilon + \epsilon^\top \boldsymbol{X}\mathbb{W}(\rho)\Delta\Phi' \\ &\quad + \Delta\Phi'^\top \mathbb{W}^\top(\rho)\boldsymbol{X}\epsilon + \epsilon^\top \boldsymbol{X}\mathbb{B}\omega + \omega^\top \mathbb{B}^\top \boldsymbol{X}\epsilon \\ &= \eta^\top \begin{pmatrix} \Omega_{11}(\rho) & \boldsymbol{X}\mathbb{W}(\rho) & \Omega_{13}(\rho) \\ \star & 0 & 0 \\ \star & \star & 0 \end{pmatrix} \eta,\end{aligned}$$

where, by using $\mathbb{A}(\rho) = A_1(\rho) + \boldsymbol{Z_1}(\rho)A_2$ then introducing the intermediate variable $\boldsymbol{Y}(\rho) = \boldsymbol{X}\boldsymbol{Z_1}(\rho)$, we obtain $\Omega_{11}(\rho) = A_1^\top(\rho)\boldsymbol{X} + \boldsymbol{X}A_1(\rho) + A_2^\top \boldsymbol{Y}^\top(\rho) + \boldsymbol{Y}(\rho)A_2$ and $\Omega_{13}(\rho) = \boldsymbol{X}B_1(\rho) + \boldsymbol{Y}(\rho)B_2$. The condition (10) gives

$$\Delta\Phi'^\top \Delta\Phi' \le \epsilon^\top \mathbb{C}^\top(\rho)\Gamma'^\top \Gamma'\mathbb{C}(\rho)\epsilon, \qquad \forall \rho \in \mathcal{P}. \tag{36}$$

This condition (independent of ω) is then re-written as $\eta^\top \mathcal{Q}(\rho)\eta \le 0$ for all $\rho \in \mathcal{P}$, where $\mathcal{Q}(\rho) = \begin{pmatrix} -\mathbb{C}^\top(\rho)\Gamma'^\top\Gamma'\mathbb{C}(\rho) & 0 & -\mathbb{C}^\top(\rho)\Gamma'^\top\Gamma'\mathbb{D}(\rho) \\ \star & I & 0 \\ \star & \star & -\mathbb{D}^\top(\rho)\Gamma'^\top\Gamma'\mathbb{D}(\rho) \end{pmatrix}$.

The $\mathcal{H}_\infty$ condition imposes that

$$\dot{V}(\eta,\rho) + e_f^\top e_f - \boldsymbol{\gamma^2}\omega^\top\omega < 0, \qquad \forall \rho \in \mathcal{P}.$$

Using the $\mathcal{S}$-procedure (Boyd et al., 1994), this is satisfied if there exists a scalar $\boldsymbol{\kappa} > 0$ such that for all $\rho \in \mathcal{P}$, $\dot{V}(\eta,\rho) + e_f^\top e_f - \boldsymbol{\gamma^2}\omega^\top\omega - \boldsymbol{\kappa}(\eta^\top \mathcal{Q}(\rho)\eta) < 0$, which is equivalent to

$$\begin{pmatrix} \Omega'_{11}(\rho) & \boldsymbol{X}\mathbb{W}(\rho) & \Omega'_{13}(\rho) \\ \star & -\boldsymbol{\kappa}I & 0 \\ \star & \star & \Omega'_{33}(\rho) \end{pmatrix} < 0, \quad \forall \rho \in \mathcal{P}, \tag{37}$$

where we use $\Omega'_{11}(\rho) = \Omega_{11}(\rho) + \mathbb{C}^\top(\rho)C_w^\top C_w\mathbb{C}(\rho) + \boldsymbol{\kappa}\mathbb{C}^\top(\rho)\Gamma'^\top\Gamma'\mathbb{C}(\rho)$, and $\Omega'_{13}(\rho) = \boldsymbol{X}B_1(\rho) + \boldsymbol{Y}(\rho)B_2 + \mathbb{C}^\top(\rho)C_w^\top C_w\mathbb{D}(\rho) + \boldsymbol{\kappa}\mathbb{C}^\top(\rho)\Gamma'^\top\Gamma'\mathbb{D}(\rho)$, and $\Omega'_{33}(\rho) = \mathbb{D}^\top(\rho)C_w^\top C_w\mathbb{D}(\rho) - \boldsymbol{\gamma^2}I + \boldsymbol{\kappa}\mathbb{D}^\top(\rho)\Gamma'^\top\Gamma'\mathbb{D}(\rho)$.
The Schur's lemma is applied to this inequality, which corresponds to the LMI (35) (when $\boldsymbol{\kappa}$ is fixed).

It is worth noting that this LMI problem is infinite-dimensional due to the dependence on the full parameter vector ρ. To make it tractable, the LMI problem (35) is to be solved only at the vertices $\varrho_i, i = 1,2,3,4$ of the polytope formed by the variation of ρ in $\mathcal{P}$, obtaining the observer matrices at these vertices denoted $\mathcal{O}(\varrho_i)$. This is possible since system $\mathcal{S}'(\rho)$ in (9), thanks to $A'(\rho)$ and $B'(\rho)$ being affine in ρ, can be expressed as a convex combination of its vertex values as

$$\mathcal{S}'(\rho) = \sum_{i=1}^{4} \sigma_i(\rho)\mathcal{S}'(\varrho_i), \quad \sigma_i(\rho) \ge 0, \quad \sum_{i=1}^{4} \sigma_i(\rho) = 1, \tag{38}$$

where $\sigma_i, i = 1,2,3,4$ are scheduling functions.

Finally, the $\mathcal{H}_\infty$ performance is implied from (37), which is $\|e_f(t)\|_{\mathcal{L}_2}^2 < \boldsymbol{\gamma^2}\|\omega(t)\|_{\mathcal{L}_2}^2$ for all $\rho \in \mathcal{P}$. ■

Remark 4. In the implementation stage, the matrices of observer $\mathcal{O}(\rho)$ in (11) are scheduled accordingly as the convex combinations:

$$\mathcal{O}(\rho) = \sum_{i=1}^{4} \sigma_i(\rho)\mathcal{O}(\varrho_i), \quad \sigma_i(\rho) \ge 0, \quad \sum_{i=1}^{4} \sigma_i(\rho) = 1. \tag{39}$$

Moreover note that, while here parameter-dependent matrices $\boldsymbol{Z_1}(\rho)$ and $\boldsymbol{Z_2}(\rho)$ are chosen for generality, they can be more conservatively taken as constants as long as the LMI in Theorem 1 is satisfied. In this case, the observer does not depend on the parameter vector.

4.2 Grid-based Design

We now propose an alternative design using *gridding*, or grid-based LMI solving and implementation. In this approach, the LMIs are not solved at the vertices of the polytope formed by ρ, but instead simply solved at the gridded values of $\rho \in \mathcal{P}$. The argument following (Wu, 1995) is that, if the rate of ρ is bounded, satisfying the LMIs at a high enough finite number of grid points implies

satisfying them at all the infinite number of points in $\mathcal{P}$. A parameter-dependent Lyapunov function can then be used, which helps relax conservativeness. For this method, the following assumption on the parameter's variation rate is needed (Wu, 1995).

Assumption 1. Assume that there exist constants $\nu_1 > 0$ and $\nu_2 > 0$ such that $|\dot{\rho}_1| \leq \nu_1$ and $|\dot{\rho}_2| \leq \nu_2$ at all times.

Theorem 2 below proposes an LMI framework for the grid-based observer design.

Theorem 2. Suppose Assumption 1 holds. The grid-based reduced-order observer design problem is solved if given some $\boldsymbol{\kappa} > 0$, there exist matrices $\boldsymbol{X}(\rho) = \boldsymbol{X}^\top(\rho) > 0$, $\boldsymbol{Y}(\rho)$, $\boldsymbol{Z_2}(\rho)$, all continuous on $\mathcal{P}$, minimizing $\boldsymbol{\gamma^2}$ such that for all grid points $\varrho_i \in \mathcal{P}$, $i = 1, 2, \ldots, n$ for some finite sufficiently large n,

$$\begin{pmatrix} \Omega_{11,\pm}(\varrho_i) & \boldsymbol{X}(\varrho_i)\mathbb{W}(\varrho_i) & \Omega_{13}(\varrho_i) & \Omega_{14}(\varrho_i) & \Omega_{15}(\varrho_i) \\ \star & -\boldsymbol{\kappa} I & 0 & 0 & 0 \\ \star & \star & -\boldsymbol{\gamma^2} I & \Omega_{34}(\varrho_i) & \Omega_{35}(\varrho_i) \\ \star & \star & \star & -I & 0 \\ \star & \star & \star & \star & -\boldsymbol{\kappa} I \end{pmatrix} < 0, \tag{40a}$$

where

$$\Omega_{11,\pm}(\varrho_i) = A_1^\top(\varrho_i)\boldsymbol{X}(\varrho_i) + \boldsymbol{X}(\varrho_i)A_1(\varrho_i) + A_2^\top \boldsymbol{Y}^\top(\varrho_i) + \boldsymbol{Y}(\varrho_i)A_2 \pm \left(\nu_1 \frac{\partial X}{\partial \rho_1}(\varrho_i) + \nu_2 \frac{\partial X}{\partial \rho_2}(\varrho_i)\right), \tag{40b}$$

$$\Omega_{13}(\varrho_i) = \boldsymbol{X}(\varrho_i)B_1(\varrho_i) + \boldsymbol{Y}(\varrho_i)B_2, \tag{40c}$$

$$\Omega_{14}(\varrho_i) = C_1^\top C_w^\top + C_2^\top \boldsymbol{Z_2}^\top(\varrho_i)C_w^\top, \tag{40d}$$

$$\Omega_{15}(\varrho_i) = \boldsymbol{\kappa}(C_1^\top \Gamma'^\top + C_2^\top \boldsymbol{Z_2}^\top(\varrho_i)\Gamma'^\top), \tag{40e}$$

$$\Omega_{34}(\varrho_i) = D_1^\top C_w^\top + D_2^\top \boldsymbol{Z_2}^\top(\varrho_i)C_w^\top, \tag{40f}$$

$$\Omega_{35}(\varrho_i) = \boldsymbol{\kappa}(D_1^\top \Gamma'^\top + D_2^\top \boldsymbol{Z_2}^\top(\varrho_i)\Gamma'^\top). \tag{40g}$$

Then, $\boldsymbol{Z_1}(\rho)$ at each grid point is $\boldsymbol{Z_1}(\varrho_i) = \boldsymbol{X}^{-1}(\varrho_i)\boldsymbol{Y}(\varrho_i)$.

Sketch-of-proof. We consider the parameter-dependent Lyapunov function $V(\epsilon, \rho) = \epsilon^\top \boldsymbol{X}(\rho)\epsilon$, where $\boldsymbol{X}(\rho) = \boldsymbol{X}^\top(\rho) > 0$ for all $\rho \in \mathcal{P}$. We then proceed similarly to the proof of Theorem 1. Note that when taking the derivative of $V(\epsilon, \rho)$, the time variation of ρ appears in the form of $\dot{\rho}$, and under Assumption 1, it is sufficient to consider in the LMIs in Theorem 2 the bounds ν_1, ν_2 in place of $\dot{\rho}_1$ and $\dot{\rho}_2$, respectively (Wu, 1995). ■

Implementation-wise, the observer matrices can be scheduled using lookup tables as in (Tran et al., 2022), from their gridded values computed from (18) and (25)-(28) by the obtained gridded values of $\boldsymbol{Z_1}(\rho)$.

5. OBSERVER SYNTHESIS AND SIMULATION

The two observers in Section 4 are designed for the SA suspension described in Section 2. Note that the parameters correspond to GIPSA-Lab's 1/5th-scale testbed (Pham et al., 2019). Note also that the grid-based design in Section 4.2 comes with an extra Assumption 1, so it cannot be justified when ρ varies infinitely fast, for example when a Skyhook controller is used (see scenario 2 below). For grid-based LMI solving, the range $\mathcal{P} := \left[\frac{1}{\overline{m}_s}, \frac{1}{\underline{m}_s}\right] \times [0, 1]$ is evenly gridded into 5 points for each parameter, so 25 points in total. In simulation, we use a sampling time of $T_s = 0.005$s, therefore we take $\nu_1 = \left(\frac{1}{\underline{m}_s} - \frac{1}{\overline{m}_s}\right)/T_s = 7.5758\text{kg}^{-1}\text{s}^{-1}$ and $\nu_2 = (1-0)/T_s = 200\text{s}^{-1}$.

5.1 Frequency-domain Analysis

In Figure 3, we show the Bode plots of only the last component of the error (29), frozen at the 25 grid points of the grid-based design, which corresponds to damper fault estimation with respect to $\dot{z}_r$. Similar plots for the polytopic design, taken at the four vertices of $\mathcal{P}$, are shown in Figure 4. It is seen that both designs provide satisfactory attenuation of the disturbance (below -50dB). Without any rigorous proof, the grid-based one is more effective in LMI solving since the parameter-dependent Lyapunov function helps to reduce conservativeness.

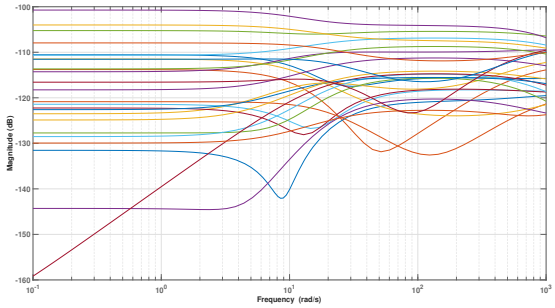

Fig. 3. $\left|\frac{f-\hat{f}}{\dot{z}_r}\right|$; *grid-based* design; 25 frozen grid points.

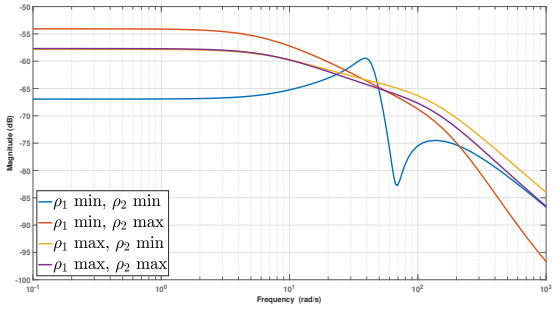

Fig. 4. $\left|\frac{f-\hat{f}}{\dot{z}_r}\right|$; *polytopic* design; four vertices.

5.2 Time-domain Simulations with the Polytopic Design

In this part, we provide some simulation results, assuming that the fault $f = \alpha F_d$ where $\alpha \in [0, 1)$ is the loss-of-efficiency factor (see Remark 2). Only the polytopic design is shown since the grid-based design cannot be applied to the case when $\rho_2 = u$ may vary infinitely fast (as the SkyHook control in the second scenario), since it violates Assumption 1. Two scenarios are illustrated as follows.

Scenario 1: Constant sprung mass and control input

- The road profile z_r is sinusoidal;
- The mass m_s is constant at 2.27kg;
- The control u is constant at $u = 0.3$;
- The factor α increases from 0.1 to 0.5 at 5s.

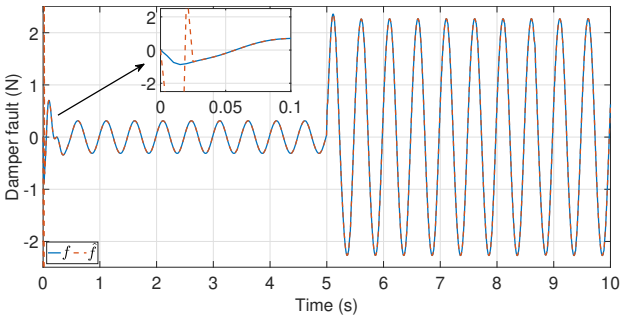

Fig. 5. Fault estimation results in scenario 1.

Scenario 2: Varying sprung mass and control input

- The road profile z_r is an ISO 8608 one of type C;
- The mass m_s increases from 2.32kg to 2.35kg at 3s;
- The control u is given by a Skyhook controller. Here, u varies infinitely fast, justifying the polytopic design;
- The factor α increases from 0.2 to 0.4 at 7s.

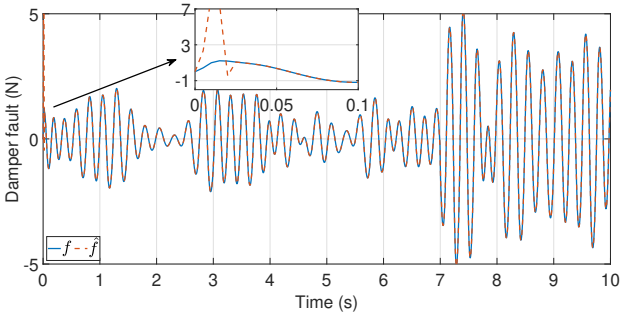

Fig. 6. Fault estimation results in scenario 2.

From Figures 5 and 6, we see that our observer provides satisfactory estimation performance. Here, the fault varies quite fast in time, so the PI observers are not justifiable.

6. CONCLUSION

This paper extends fault estimation observer designs, namely the polytopic and grid-based designs of the reduced-order descriptor observer, for the SA suspension in the case of a varying sprung mass that is highly practical. The designs are analyzed via Bode plots and time simulations. These results illustrate the effectiveness of the polytopic design for damper fault estimation. Future work is to take *uncertainty* in vehicle mass measurement/estimation into account for even higher practicality.

REFERENCES

Boyd, S., El Ghaoui, L., Feron, E., and Balakrishnan, V. (1994). *Linear matrix inequalities in system and control theory*. SIAM.

Darouach, M., Amato, F., and Alma, M. (2017). Functional observers design for descriptor systems via LMI: Continuous and discrete-time cases. *Automatica*, 86, 216–219.

Delshad, S.S., Johansson, A., Darouach, M., and Gustafsson, T. (2016). Robust state estimation and unknown inputs reconstruction for a class of nonlinear systems: Multiobjective approach. *Automatica*, 64, 1–7.

Do, M.H., Koenig, D., and Theilliol, D. (2020). Robust observer-based controller for uncertain-stochastic linear parameter-varying (LPV) system under actuator degradation. *Int. J. of Robust Nonlin. Control*, 31, 662 – 693.

Do, M.H., Koenig, D., and Theilliol, D. (2018). Robust H∞ proportional-integral observer for fault diagnosis: application to vehicle suspension. *IFAC-POL*, 51(24), 536–543.

Gobbi, M., Mastinu, G., and Previati, G. (2011). A Method for measuring the inertia properties of rigid bodies. *Mech. Syst. and Signal Proc.*, 25(1), 305–318.

Guzman, J., López-Estrada, F.R., Estrada-Manzo, V., and Valencia-Palomo, G. (2021). Actuator fault estimation based on a proportional-integral observer with non-quadratic Lyapunov functions. *Int. J. of Syst. Sci.*, 1–14.

Hernández-Alcántara, D., Tudón-Martínez, J.C., Amézquita-Brooks, L., Vivas-López, C.A., and Morales-Menéndez, R. (2016). Modeling, diagnosis and estimation of actuator faults in vehicle suspensions. *Control Engineering Practice*, 49, 173–186.

Isermann, R. (2005). *Fault-diagnosis Systems: An Introduction from Fault Detection to Fault Tolerance*. Springer Science & Business Media.

Maciejewski, I., Glowinski, S., and Krzyzynski, T. (2014). Active control of a seat suspension with the system adaptation to varying load mass. *Mechatronics*, 24(8), 1242–1253.

Morato, M., Pham, T.P., Sename, O., and Dugard, L. (2020). Development of a simple ER damper model for fault-tolerant control design. *J. of the Brazilian Soc. of Mech. Sci. and Eng.*, 42(10), 502 (2020).

Pham, T.P., Sename, O., and Dugard, L. (2019). Unified $\mathcal{H}_\infty$ observer for a class of nonlinear Lipschitz systems: application to a real ER automotive suspension. *IEEE Control Systems Letters*, 3(4), 817–822.

Pham, T.P., Sename, O., and Tran, G.Q.B. (2022). Non linear parameter varying observer based on descriptor modeling for damper fault estimation. *IFAC-POL*, 55(35), 91–96.

Savaresi, S.M., Poussot-Vassal, C., Spelta, C., Sename, O., and Dugard, L. (2010). *Semi-active suspension control design for vehicles*. Elsevier.

Tran, G.Q.B., Pham, T.P., and Sename, O. (2022). Multi-objective grid-based Lipschitz NLPV PI observer for damper fault estimation. *IFAC-POL*, 55(6), 163–168.

Tudón-Martínez, J.C., Hernández-Alcántara, D., and Morales-Menendez, R. (2015). Semi-active suspension control with LPV mass adaptation. *IFAC-POL*, 48(26), 67–72.

Unger, A., Schimmack, F., Lohmann, B., and Schwarz, R. (2013). Application of LQ-based semi-active suspension control in a vehicle. *Control Engineering Practice*, 21(12), 1841–1850.

Wen, S., Chen, M.Z.Q., Zeng, Z., Yu, X., and Huang, T. (2017). Fuzzy control for uncertain vehicle active suspension systems via dynamic sliding-mode approach. *IEEE Trans. on Syst. Man Cyber.: Syst.*, 47(1), 24–32.

Wenzel, T.A., Burnham, K.J., Blundell, M.V., and Williams, R.A. (2006). Dual extended Kalman filter for vehicle state and parameter estimation. *Vehicle System Dynamics*, 44(2), 153–171.

Wu, F. (1995). *Control of linear parameter varying systems*. Ph.D. thesis, University of California, Berkeley.